ChemComm

COMMUNICATION

View Article Online
View Journal | View Issue

Check for updates

Cite this: *Chem. Commun.*, 2023, 59, 8544

Received 1st May 2023,
Accepted 6th June 2023

DOI: 10.1039/d3cc02094k

rsc.li/chemcomm

Published on 06 Juni 2023. Downloaded on 13.02.2026 11:29:02.

Ionic liquid enables high-performance, self-powered $CsPbBr_3$ perovskite nanonet photodetector†

Hai Zhou, *[abc] Rui Wang,[ac] Xuhui Zhang,[ac] Bo'ao Xiao,[ac] Zihao Shuang,[a] Dingjun Wu[a] and Pingli Qin*[b]

We fabricated high-quality $CsPbBr_3$ perovskite nanonet films with the assistance of polystyrene spheres, and constructed self-powered photodetectors (PDs) with an ITO/SnO_2/$CsPbBr_3$/carbon structure. By passivating the nanonet with different concentrations of 1-butyl-3-methylimidazolium bromide (BMIMBr) ionic liquid, we found that as the concentration of BMIMBr increases, the dark current of the device first decreases and then gradually increases, while the photocurrent remains essentially unchanged. Finally, the PD with 1 mg mL^{-1} BMIMBr ionic liquid exhibited the best performance with a switch ratio of about 1.35×10^6, a linear dynamic range extending to 140 dB, and responsivity and detectivity values of 0.19 A W^{-1} and 4.31×10^{12} Jones, respectively. These results provide an important reference for fabricating perovskite PDs.

$CsPbBr_3$ perovskite not only has the unique advantages of the perovskite family, such as simple preparation process and high charge carrier mobility, its all-inorganic structure is more stable than those of organic–inorganic and two-dimensional perovskites, showing great potential in fields such as solar cells, PDs, and light-emitting diodes.[1–5] However, the rapid solvent evaporation and crystallization during the preparation of perovskite films usually result in poor crystallinity, high defect density, pinholes, and small grain size, which decrease the performance and stability of perovskite PDs.[6,7] Therefore, controlling the crystallization rate of $CsPbBr_3$ perovskite has become an effective means of improving the quality of its films.[7–9] In addition, severe charge recombination processes take place at the interface of the device and the grain boundaries of perovskite crystals, which result in the degradation of device performance. Therefore, passivating the defects of the perovskite absorber layer is also a key factor in improving the performance of perovskite optoelectronic devices.[10–17]

Ionic liquids, as an excellent type of material, have been reported to efficiently passivate the defects of perovskites[18–22] due to the existence of BMIMBr, which can passivate the related deep traps induced by the halide in $CsPbBr_3$ because the positive electron density of the organic cation $[BMIM]^+$ can acquire electrons from the under-coordinated Br^- and the Pb–Br antisite defects ($PbBr_3^-$). Besides, the high negative electron density of the inorganic anion $[BBr_4]^-$ enables its incorporation into the lattice structure of $CsPbBr_3$ to compensate Br vacancies and passivate unsaturated-Pb-related defects in $CsPbBr_3$. More importantly, ionic liquids show many advantages: (1) they contain a large number of asymmetric organic cations, such as imidazole, phosphorus, and pyridine, which combine with organic or inorganic anions of opposite polarity, such as $COOH^-$, CF_3COO^-, BF_4^-, Cl^-, and I^-; (2) ionic liquids are composed entirely of ions, so they have good conductivity and thermal stability, as well as good solubility, low toxicity, and low flammability, making them an ideal material for optoelectronic passivation; (3) ionic liquids are hydrophobic, so using them as additives is an effective way of adjusting the hydrophobicity of precursor solutions and prevent water penetration.

Owing to the advantages of high-quality film formation based on crystal growth rate control and efficient passivation of defects by ionic liquids, we have employed polystyrene (PS) spheres as a template to control the crystallization rate of the perovskite for fabricating high-quality $CsPbBr_3$ perovskite nanonet films, and then 1-butyl-3-methylimidazolium bromide (BMIMBr ionic liquid) is chosen for passivating the $CsPbBr_3$ perovskite nanonet with different concentrations due to its great improvement to our device performance and stability in our previous work[20,21], and finally a self-powered PD with an ITO/SnO_2/$CsPbBr_3$/carbon structure is constructed. By analyzing the photo/dark current of the PDs passivated with different concentrations of BMIMBr ionic liquid, it was found that as the concentration of BMIMBr ionic liquid increased, the dark

[a] *International School of Microelectronics, Dongguan University of Technology, Dongguan, Guangdong, 523808, China. E-mail: hizhou@dgut.edu.cn*
[b] *Hubei Key Laboratory of Optical Information and Pattern Recognition, Wuhan Institute of Technology, Wuhan, 430205, China. E-mail: qpl2015@wit.edu.cn*
[c] *Faculty of Physics & Electronic Science, Hubei University, Wuhan, 430062, China*

† Electronic supplementary information (ESI) available. See DOI: https://doi.org/10.1039/d3cc02094k

This journal is © The Royal Society of Chemistry 2023

Published on 06 Juni 2023. Downloaded on 13.02.2026 11:29:02.

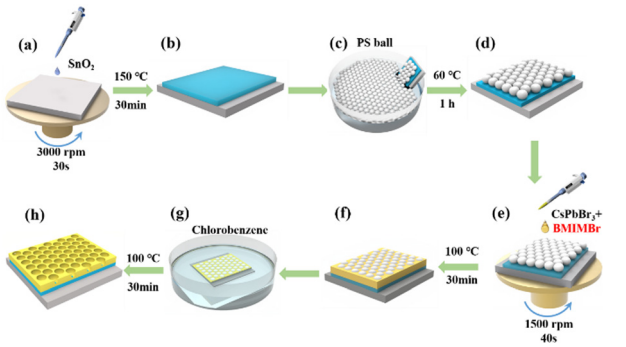

Fig. 1 Schematic diagram of the fabrication process for the $CsPbBr_3$ perovskite nanonet.

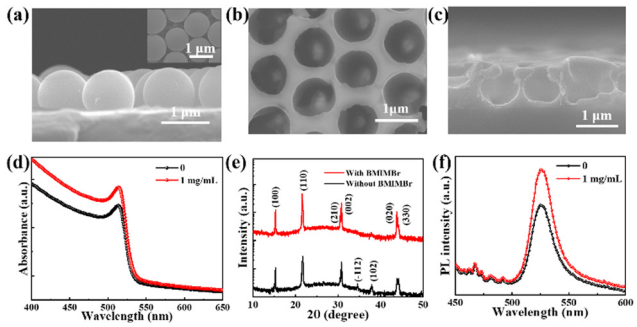

Fig. 2 (a) Cross-sectional SEM image of single-layer PS spheres; the inset shows the top view SEM image of single-layer PS spheres. Top (b) and cross-sectional (c) SEM image of the $CsPbBr_3$ perovskite nanonet film with BMIMBr ionic liquid. (d) Absorption spectra of the $CsPbBr_3$ perovskite nanonet films. (e) XRD patterns of the $CsPbBr_3$ perovskite nanonet films. (f) Steady-state PL spectra of the $CsPbBr_3$ perovskite nanonet films.

current of the device first decreased and then gradually increased, while the photocurrent remained essentially unchanged. Finally, the device containing 1 mg mL^{-1} BMIMBr ionic liquid displayed the best performance, achieving a switch ratio of approximately 1.35×10^6, an impressive linear dynamic range (LDR) of 140 dB, a responsivity (R) of 0.19 A W^{-1}, and detectivity (D^*) of 4.31×10^{12} Jones. These results provide a reference value for fabricating perovskite PDs.

A schematic diagram of the fabrication process for the $CsPbBr_3$ perovskite nanonet is presented in Fig. 1, with a more detailed description available in our previous work[23] and the experimental section. To begin with, SnO_2 solution was dispensed onto the ITO substrate that had been treated, and then spin-coated at 3000 rpm for 30 seconds. Then, single-layered PS microspheres were coated on the SnO_2/ITO substrate for the subsequent preparation of the perovskite. To investigate the effect of BMIMBr ionic liquid on the $CsPbBr_3$ perovskite nanonet PD, different concentrations of BMIMBr ionic liquid were added to the $CsPbBr_3$ precursor solution to obtain the optimal concentration. Then, the precursor solution was dropped onto a SnO_2/ITO substrate with PS spheres. The substrate was then spin-coated and annealed on a heating stage for 30 min. After that, the $CsPbBr_3$ film was submersed in a glass bottle containing chlorobenzene to eliminate the PS spheres. Finally, the carbon electrodes were fabricated on the sample surface using screen printing technology, and the $CsPbBr_3$ nanonet PDs were fabricated with an ITO/SnO_2/$CsPbBr_3$/carbon structure, and the active area of the device is 0.2×0.2 cm^2.

The SEM images in Fig. 2a depict cross-sectional and top views of single-layer PS spheres on our substrates, confirming their uniformity, and clearly showing that the PS spheres on our substrates are in a single layer. With the assistance of these single-layer PS spheres, we obtained the perovskite nanonet film, whose surface morphology is as shown in Fig. 2b while Fig. 2c shows the corresponding cross-sectional SEM image. During the experiment, it was observed that a nanonet hollow structure could be created in all $CsPbBr_3$ films, regardless of the presence or absence of the ionic liquid (as indicated in Fig. S1, ESI†), after removing the PS microspheres. Additionally, the resulting nanonet film had a thickness of approximately 1 μm. The uniformly dense nanonet can effectively reduce light reflection and improve light utilization efficiency, and provides better photoelectric detection performance.[6]

The light absorption curves of the $CsPbBr_3$ films with and without the inclusion of BMIMBr ionic liquid are presented in Fig. 2d. From the figure, the $CsPbBr_3$ film with BMIMBr ionic liquid shows a higher absorption peak, which can be attributed to the improved crystalline quality of the $CsPbBr_3$ film with the addition of BMIMBr ionic liquid. Fig. 2e shows the X-ray diffraction (XRD) patterns of $CsPbBr_3$ films with and without the addition of BMIMBr ionic liquid. From the XRD patterns, the characteristic peaks of the $CsPbBr_3$ films have higher intensity after the addition of BMIMBr, particularly the (110) peak, indicating that the fabricated $CsPbBr_3$ nanonet film after the addition of BMIMBr has higher crystal quality, which is conducive to achieving excellent device performance. The steady-state photoluminescence (PL) spectra of the $CsPbBr_3$ films are shown in Fig. 2f. Under excitation by a 320 nm laser, the $CsPbBr_3$ film incorporating BMIMBr exhibits a significantly greater PL intensity compared to that without BMIMBr, suggesting that the $CsPbBr_3$ film based on BMIMBr has reduced defect density and superior crystalline quality.[21,24]

Fig. 3a shows the schematic structure of the nanonet-structured $CsPbBr_3$ PD, which consists of ITO/SnO_2/nanonet-structured $CsPbBr_3$/carbon layers. The presence of the nanonet-structured hollow $CsPbBr_3$ film effectively increases the surface area of the film and reduces light reflection, leading to better utilization of

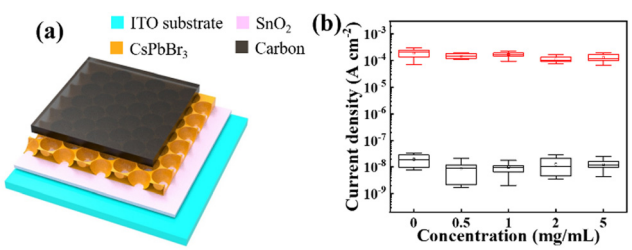

Fig. 3 (a) Schematic structure of the $CsPbBr_3$ nanonet PD. (b) Light and dark current statistics of the $CsPbBr_3$ nanonet PDs with various concentrations of BMIMBr ionic liquid.

Published on 06 Juni 2023. Downloaded on 13.02.2026 11:29:02.

light.[16] To investigate the optimal concentration of BMIMBr ionic liquid to improve the performance of the nanonet-structured $CsPbBr_3$ PDs, 0/0.5/1/2/5 mg mL^{-1} BMIMBr ionic liquid was added to the precursor solution. Good photoelectric performance was exhibited by all devices, as depicted in Fig. 3b. With the increase of the BMIMBr ionic liquid concentration, the dark current density of the devices decreased first and then gradually increased, while the photocurrent density remained almost unchanged. For the changes to the dark current density, we think the reduced dark current density is attributed to the reduction of the Br vacancies by adding BMIMBr. However, with further increasing the concentration of BMIMBr, more BMIMBr leads to more Br ions, which increases the conductivity of the device and finally increases the dark current density of the device. Compared with the devices using other concentrations of ionic liquids, the device using 1 mg mL^{-1} BMIMBr ionic liquid has the lowest dark current density, maximum photocurrent density, and more concentrated statistical data distribution with higher repeatability. Therefore, 1 mg mL^{-1} was chosen as the optimal concentration of BMIMBr ionic liquid.

The characteristic current–voltage (I–V) curves of the $CsPbBr_3$ nanonet PDs with the optimal BMIMBr ionic liquid (1 mg mL^{-1}) are shown in Fig. 4a. From the curves, the device exhibits good rectifying characteristics and has good self-powered ability, with an open-circuit voltage of 1.24 V under 145 mW cm^{-2} illumination. The current–time (I–t) curves of the $CsPbBr_3$ nanonet PDs with the optimal BMIMBr ionic liquid under different light intensities at 0 V are shown in Fig. 4b. As the light power increases from 1.45×10^{-5} to 145.8 mW cm^{-2}, the photocurrent also gradually increases, showing a positive correlation. At the same time, the dark current of the device is extremely low, at about 2.51×10^{-10} A, while the photocurrent at the maximum light power reaches 3.4×10^{-4} A, and the on–off ratio of the device can be calculated to be about 1.35×10^{6}. Besides, there is a certain fluctuation in the dark current, we think the main reason is attributed to the existence of the defect in the perovskite. When the device is illuminated by light, a large number of photo-generated carriers will be generated, and some of them may be trapped by these defects and remain. After the light is removed, these remaining photo-generated carriers will be slowly released and cause the increase of the dark current. When stronger light is applied, more photo-generated carriers are generated and more are left, resulting in the dark current fluctuating under different light intensities.

The correlation between the light intensity and photocurrent density is illustrated in Fig. 4c. By using the formula $\mathrm{LDR} = 20\log\frac{P_{\max}}{P_{\min}}$, where $P_{\max}$ ($P_{\min}$) is the incident light intensity above (below) which the photocurrent begins to deviate from linearity, the LDR of the device can be calculated with a value of up to 140 dB. In addition, by linearly fitting the data, the R-square of the device is 0.997, which is very close to 1, indicating good linearity in the measurement range. Based on the formulas $R = \frac{I_{\mathrm{ph}} - I_{\mathrm{d}}}{SL_{\mathrm{light}}}$ and $D^{*} = \frac{R\sqrt{S}}{\sqrt{2qI_{\mathrm{d}}}}$, the R and D^{*} curves are plotted in Fig. 4d, indicating a decrease in the R and D^{*} values with increasing light intensity. Under irradiation of 1.45×10^{-5} mW cm^{-2}, the maximum R and D^{*} of the device are 0.19 A W^{-1} and 4.31×10^{12} Jones (1 Jones = 1 cm $Hz^{1/2}$ W^{-1}), respectively. These values are comparable to those of the most advanced perovskite PDs (the detailed comparison is shown in Table S1, ESI†),[25–27] showing that the nanonet-structured $CsPbBr_3$ PD with the optimal BMIMBr ionic liquid concentration exhibits excellent photodetection ability.

To measure the frequency response of the device, an optical chopper was used to change the frequency of the incident light (1 Hz–10 kHz), and the resulting $f_{-3\mathrm{dB}}$ curve is depicted in Fig. 4e. As the frequency increases, the waveform gradually changes from a square wave to a triangular wave, and the $f_{-3\mathrm{dB}}$ of the device is about 4 kHz. In addition, it can be seen from the fast response I–t curve (Fig. 4f) that the rise and fall times (τ_{rise} and τ_{fall}) of the optimal BMIMBr ionic liquid concentration $CsPbBr_3$ nanonet PD are 0.06 ms and 0.26 ms, respectively, indicating a fast response speed.

In conclusion, we introduced PS spheres to assist in the preparation of high-quality $CsPbBr_3$ perovskite nanonet films, and explored the effect of different concentrations of BMIMBr ionic liquid on the performance of the nanonet-structured $CsPbBr_3$ PD. The results showed that the device with the optimal concentration of BMIMBr ionic liquid had better crystallization and optimal photoelectric performance, with a switch ratio of about 1.35×10^{6} and an LDR of 140 dB. The device reached maximum R and D^{*} values of 0.19 A W^{-1} and 4.31×10^{12} Jones, respectively, when irradiated at 1.45×10^{-5} mW cm^{-2}. These results provide a reference for fabricating perovskite PDs.

This work was supported by the National Natural Science Foundation of China (No. 51972101), the Research Platforms and Projects of Guangdong Universities in 2022 (No. 2022ZDZX1028), and Hubei Key Laboratory of Optical Information and Pattern Recognition, Wuhan Institute of Technology (No. 202206).

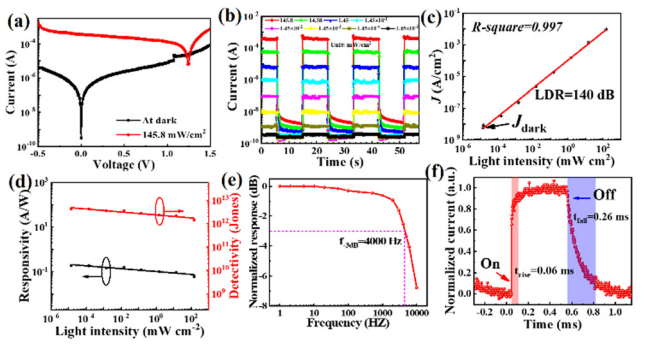

Fig. 4 The performance of the $CsPbBr_3$ nanonet PD with the optimal BMIMBr ionic liquid concentration (1 mg mL^{-1}): (a) I–V curves; (b) I–t curves at different light intensities; (c) LDR; (d) R and D*; (e) $f_{-3\mathrm{dB}}$ bandwidth; (f) response speed.

Conflicts of interest

The authors declare that they have no conflict of interest.

This journal is © The Royal Society of Chemistry 2023

Notes and references

1 C. Xie, C. K. Liu, H. L. Loi and F. Yan, *Adv. Funct. Mater.*, 2020, **30**(20), 1903907.
2 C. Xie, P. You, Z. Liu, L. Li and F. Yan, *Light Sci. Appl.*, 2017, **6**(8), e17023–e17023.
3 H. Zhou, Z. Song, C. R. Grice, C. Chen, J. Zhang, Y. Zhu, R. Liu, H. Wang and Y. Yan, *Nano Energy*, 2018, **53**, 880–886.
4 X. Pan, J. Zhang, H. Zhou, R. Liu, D. Wu, R. Wang, L. Shen, L. Tao, J. Zhang and H. Wang, *Nano-Micro Lett.*, 2021, **13**, 1–12.
5 G. Li, Y. Wang, L. Huang and W. Sun, *ACS Appl. Electron. Mater.*, 2022, **4**(4), 1485–1505.
6 R. Liu, H. Zhou, Z. Song, X. Yang, D. Wu, Z. Song, H. Wang and Y. Yan, *Nanoscale*, 2019, **11**(19), 9302–9309.
7 J. Zeng, X. Li, Y. Wu, D. Yang, Z. Sun, Z. Song, H. Wang and H. Zeng, *Adv. Funct. Mater.*, 2018, **28**(43), 1804394.
8 X. Zeng, W. Li, C. Yan, J. Cao, X. Fu and W. Yang, *J. Mater. Chem. C*, 2021, **9**(44), 15967–15976.
9 Y. Ren, Y. Hao, N. Zhang, Z. Arain, M. Mateen, Y. Sun, P. Shi, M. Cai and S. Dai, *Chem. Eng. J.*, 2020, **392**, 123805.
10 W. Zhao, P. Guo, J. Su, Z. Fang, N. Jia, C. Liu, L. Ye, Q. Ye, J. Chang and H. Wang, *Adv. Funct. Mater.*, 2022, **32**(24), 2200534.
11 J. Xu, J. Cui, S. Yang, Y. Han, X. Guo, Y. Che, D. Xu, C. Duan, W. Zhao, K. Guo and W. Ma, *Nano-Micro Lett.*, 2022, **14**(1), 7.
12 W. Dong, W. Qiao, S. Xiong, J. Yang, X. Wang, L. Ding, Y. Yao and Q. Bao, *Nano-Micro Lett.*, 2022, **14**(1), 108.
13 R. Lin, J. Xu, M. Wei, Y. Wang, Z. Qin, Z. Liu, J. Wu, K. Xiao, B. Chen, S. M. Park and G. Chen, *Nature*, 2022, **603**(7899), 73–78.
14 J. Wang, L. Liu, S. Chen, L. Qi, M. Zhao, C. Zhao, J. Tang, X. Cai, F. Lu and T. Jiu, *Small*, 2022, **18**(3), 2104100.
15 Y. He, M. Petryk, Z. Liu, D. G. Chica, I. Hadar, C. Leak and M. G. Kanatzidis, *Nat. Photonics*, 2021, **15**(1), 36–42.
16 L. Zhao, Y. Zhou, Z. Shi, Z. Ni, M. Wang, Y. Liu and J. Huang, *Nat. Photonics*, 2023, **17**(4), 315–323.
17 Y. Zhou, C. Fei, M. A. Uddin, L. Zhao, Z. Ni and J. Huang, *Nature*, 2023, 1–7.
18 F. Wang, C. Y. Ge, D. Duan, H. Lin, L. Li, P. Naumov and H. Hu, *Small Structures*, 2022, **3**(8), 2200048.
19 H. Peng, D. Li, Z. Li, Z. Xing, X. Hu, T. Hu and Y. Chen, *Nano-Micro Lett.*, 2023, **15**(1), 91.
20 Z. Gao, H. Zhou, K. Dong, C. Wang, J. Wei, Z. Li, J. Li, Y. Liu, J. Zhao and G. Fang, *Nano-Micro Lett.*, 2022, **14**(1), 215.
21 D. Wu, Y. Xu, H. Zhou, X. Feng, J. Zhang, X. Pan, Z. Gao, R. Wang, G. Ma, L. Tao, H. Wang, J. Duan, H. Wan, J. Zhang, L. Shen, H. Wang and T. Zhai, *InfoMat*, 2022, **4**(9), e12320.
22 L. Gu, C. Ran, L. Chao, Y. Bao, W. Hui, Y. Wang, Y. Chen, X. Gao and L. Song, *ACS Appl. Mater. Interfaces*, 2022, **14**(20), 22870–22878.
23 R. Wang, H. Zhou, B. Wu, D. Wu, L. Tao, H. Wang, X. Peng, J. Zhang and H. Wang, *J. Phys. Chem. Lett.*, 2021, **12**(31), 7519–7525.
24 M. Du, X. Zhu, L. Wang, H. Wang, J. Feng, X. Jiang, Y. Cao, Y. Sun, L. Duan, Y. Jiao, K. Wang, X. Ren, Z. Yan, S. Pang and S. Liu, *Adv. Mater.*, 2020, **32**(47), 2004979.
25 Z. Shuang, H. Zhou, D. Wu, X. Zhang, B. Xiao, G. Ma, J. Zhang and H. Wang, *Chem. Eng. J.*, 2022, **433**, 134544.
26 J. Yan, Y. Li, F. Gao, W. Gong, Y. Tian and L. Li, *J. Mater. Chem. C*, 2022, **10**(23), 8922–8930.
27 W. Kim, J. Park, Y. Aggarwal, S. Sharma, E. H. Choi and B. Park, *Nanomaterials*, 2023, **13**(3), 619.

Published on 06 Juni 2023. Downloaded on 13.02.2026 11:29:02.